



Multi-Fidelity Shape Optimization of a High Lift Reentry Vehicle for a Suborbital Reentry Mission

Fynn Barz¹

Abstract

In the present study, the multi-fidelity shape optimization of a high lift re-entry vehicle is investigated. The vehicle shape is optimized for a cruise flight mission with the lift to drag ratio as objective function. The constraints in the vehicles design parameter prevent non-realistic configurations. The optimization is performed by a surrogate based optimization with an inner and outer loop. The inner loop optimizes the flight attitude, the angle of attack and flap deflection for maximum lift to drag ratio. The outer loop finds the best design parameter combination. The hierarchical kriging is used for the multi-fidelity optimization. Within the optimization, the fidelity of the aerodynamic calculation is varied. The low-fidelity aerodynamic solution is calculated by the shock expansion method whereas the higher-fidelity level is generated by Euler calculations.

Nomenclature

| Abbreviations | | Latin | |
|---------------|---|---------------------|-----------------------------|
| | | b | Wing Bending |
| CFD | Computational Fluid Dynamics | C_m | Pitching Moment Coefficient |
| DLR | German Aerospace Center | g_f | Flap Gap |
| HDF5 | Hierarchical Data Format 5 | i_o | Outer Iteration |
| HLRV | High Lift Re-entry Vehicle | l | Vehicle Length |
| IGES | Initial Graphics Exchange Specification | L/D | Lift to Drag Ratio |
| SBO | Surrogate Based Optimization | l_f | Flap Start Position |
| SMARTy | Surrogate Modeling for Aero-Data Tool- | M | Mach Number |
| | box in python | M_d | Design Mach Number |
| WR | Waverider | n | Number of Mesh Points |
| Subscripts | | s | Half Span Width |
| lee | Lee Side | s_{fi} | Inner Flap Edge |
| luv | Luv Side | s_{fo} | Outer Flap Edge |
| Greek | | t_f | Flap Thickness |
| α | Angle of Attack | Superscr | ipts |
| δ | Flap Deflection | * | Output Value |
| θ | Semi-Vertical Shock Angle | $	ilde{y},	ilde{z}$ | Normalized Coordinates |

¹German Aerospace Center (DLR), Institute of Aerodynamics and Flow Technology, Spacecraft, Lilienthalplatz 7, 38108 Braunschweig, Germany, fynn.barz@dlr.de

1. Introduction

The re-entry of vehicle from space missions is a complex task due to the wide range of speeds and varying altitude. According to this, the design problem is a multidisciplinary problem. In the last years, the interest of reusable systems for space transportation increased. This can be seen by the successful operation of the SpaceX Falcon 9 booster. A winged first stage concept as competitor is shown by the DLR [12]. The wings result in increased lift and thus higher maneuverability. This makes winged re-entry vehicles aside of civil purposes of special interest from a defense perspective.

The above-mentioned multidisciplinary problem makes an optimization very computationally costly. Therefore, in literature, the idea arises to perform optimization with multi-fidelity levels for complex problems. This means the model directly takes the low-fidelity solution as a trend for the high-fidelity model [5]. The multi-fidelity optimization was recently, successfully applied for aerodynamic problems. The optimization of a high-lift and cruise airfoil was shown by Kontogiannis [6]. The resulting airfoils, optimized by the multi-fidelity approach, showed a mature result due to the high-fidelity computations within the optimization.

Furthermore, a transonic compressor rotor was optimized by Mondal [8] with a machine learning enhancement of the SBO within the multi-fidelity optimization. The application for an Orion-like capsule re-entry was demonstrated by Di Fiore [3] where multi-fidelity domain-aware learning was used. The method showed superior results compared with a single-fidelity optimization.

The objective of this study is to show the leverage of the multi-fidelity optimization for a WR-like re-entry vehicle. Here, the focus is on the single discipline optimization, the aerodynamics. Stacked multi-fidelity SBO are utilized for the shape optimization of a WR. The vehicle is optimized for a cruise flight with constant speed of M=10. The lift to drag ratio is the objective function for the SBO. The constraint for a feasible vehicle is the trim ability of the WR. This can be achieved by deflecting flaps in the rear of the vehicle. The volume of the geometry is constrained by the design parameter of the WR.

2. Numerical Setup

In the following sections the numerical setup of the components of the optimization are described: the design of the geometry, the aerodynamic solver and the optimization itself.

2.1. Geometry Design

Waverider shapes are designed inversely. The basis is a inviscid flow field behind a compression shock generated by a slender body. The luv-surface of the vehicle is formed by a surface generated by streamlines beginning at the shock. The method used here is the osculating cone method [10]. Within this method, the flow field is defined as series of 2d flow fields calculated by the Taylor-Maccoll-equation forming a 3d flow field. This increases the flexibility of designing waverider shapes due to the ability of defining various shock shapes. The waverider investigated here, is generated by a cone shock of the radius R=2.3, a semi-vertical shock angle of $\theta=10^\circ$ and a design Mach number $M_d \in [8,14]$. The luv-surface shape is further defined by a line in the rear plane. The line is named luv line, see Fig 1, from which the streamlines are traced until they reach the shock. For the optimization, this line is defined as a straight line towards 70% of the half wingspan. Thereafter, the bending of the wing tip is described by a quadratic function, as defined in Eq 1

$$f(\tilde{y}) = b\left(\tilde{y} - 0.7\right)^2 \tag{1}$$

with a scaling factor b, hereafter wing bending, which is varied between $b \in [-0.6, 0.6]$.

Control surfaces are integrated in the rear of the vehicle for trimming, see Fig 2. The surfaces are flaps on the luv- and lee-side which can be deflected outwards. The flap size is defined relative to the length l and half span width s of the WR. The flaps start, beginning from the nose, at $l_f=0.9l$. In the span-wise direction, the inner flaps edge is at $s_{fi}=0.1s$ and the outer edge at $s_{fo}=0.5s$. For the higher fidelity calculations, the flap needs to be cut out of the WR geometry with a thickness of $t_f=0.01l$. The by of the flap is generated with a gap of $g_f=0.2t_f$.

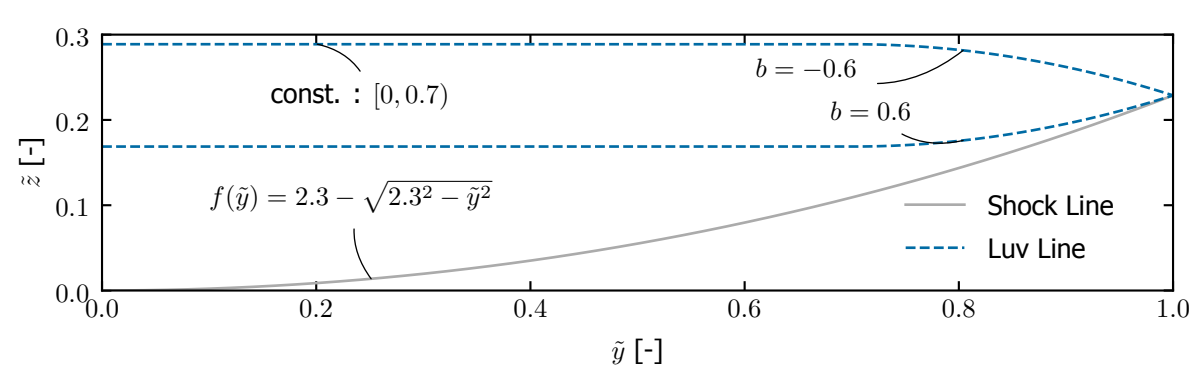


Fig 1. The shock- and luv-line for the definition of the WR shape. The luv-lines for the minimum and maximum wing bending are shown.

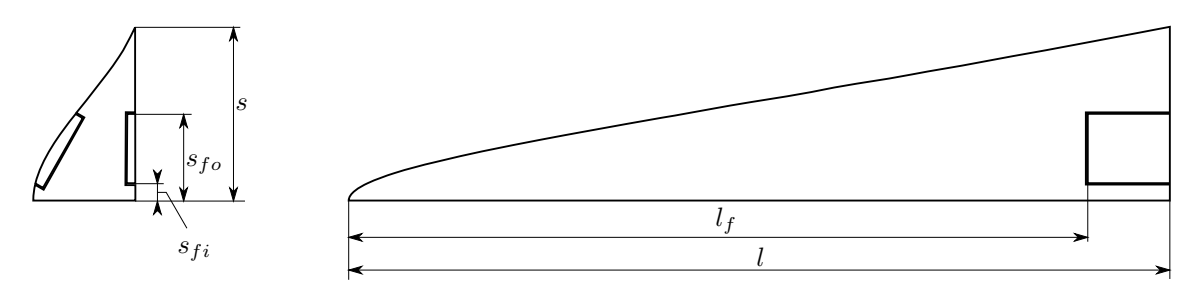


Fig 2. The dimension of the flaps on the example of the WR with the parameter b=0 and $M_d=11$.

2.2. Aerodynamic Solver

The aerodynamic within the optimization is calculated by two level of fidelity. The low-fidelity aerodynamic is calculated by the shock expansion method [1]. The shock-expansion-method is a local panel method. This means, the local flow state and geometrical properties of the local panel are taken into account only. In an iterative process, starting with the leading edge, the flow state on every panel is calculated downstream. The initial state at the leading edge position is described by the oblique shock relations from free stream. Continuing downstream by conducting the Prandtl-Meyer-Expansion for local panel deflections which are backward facing and the oblique shock relations for forward facing deflections to calculate the next downstream panels state.

The method is valid for WR shaped vehicles due to their slender shape. The slenderness reduces the influence of disturbances reflected by the compression shock. Furthermore, Franze et al. [4] showed a comparison of multiple local inclination methods against high-fidelity calculations performed with non-equilibrium gas RANS calculations. The results highlight, that errors of 10% and less for the lift, drag and pitching moment along the whole re-entry trajectory could be reached. Thus, the method gives a good trend for the higher fidelity solution.

For the higher fidelity, the TAU solver [9] is used to perform Euler calculations. The mesh is an unstructured tetrahedron mesh. The deflection of the flaps is realized by rotation w.r.t. the hinge line and complete re-meshing. The time consumption for the re-meshing is less than using overlapping meshes due to the high number of points needed in the overlap region. The half model is used to further reduce the number of points.

Following the mesh convergence for the pitching moment coefficient C_m and the lift to drag ratio L/D is shown, see Fig 3. Here, the configuration in the center of the design space with a wing bending of b=0 and a design mach number of $M_d=11$ is calculated. The flaps are not deflected. The number of points range from $n\approx 12\,\mathrm{k}$ to $n\approx 1.9\,\mathrm{m}$. In the figure, a band of $\pm 5\%$ of result of the finest mesh is depicted. It can be see, the mesh with $n\approx 471\,\mathrm{k}$ points is in the band and thus used for further

calculations.

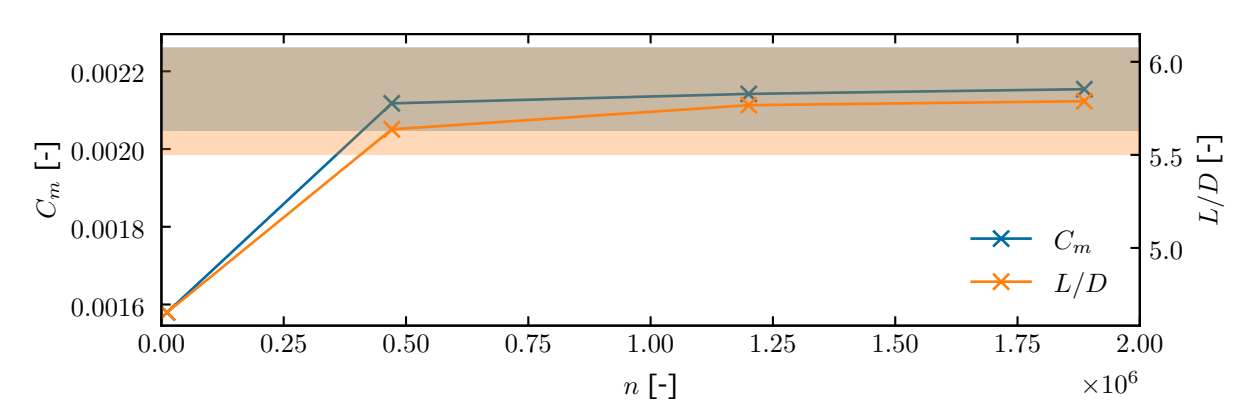


Fig 3. The convergence of the pitching moment coefficient C_m and the lift to drag ratio L/D over number of mesh points n. A band of $\pm 5\%$ is depicted w.r.t. the value of the finest mesh.

2.3. Optimization

The optimization is performed within the SMARTy framework which stands for Surrogate Modeling for Aero-Data Toolbox in python [2]. The framework provides various data-driven models to incorporate data of different sources from e.g. handbook methods to flight test data. Within this work, the surrogate based optimization (SBO) is used which enables the global optimization of complex engineering designs. This is due to the surrogate which represents an approximation of the relation between the design parameters and the quantity of interest by simpler mathematical models. Another advantage is the usage of e.g. Gaussian processes as mathematical model which intrinsically approximate response and errors.

The SBO can be divided in three steps. In the first step, the design of experiment is created which is the matrix of parameter. Within the design of experiment, the Sobol's sequence [11] is used to initially sample parameter combinations. The number of initial sampling points is set to 10 times the design parameter dimension [7] The objective function is evaluated for the sampled combinations as initial data for the surrogate model. Here, kriging is used as surrogate with a Gaussian kernel. Second, the surrogate model with the initial data is conducted to add additional data points. The surrogate provides the normal distribution prediction of the objective function and thus, the probability of the sample with the best improvement of the model can be evaluated. The method is named expected improvement which improves the whole domain of the surrogate. Due to the improvement in the whole domain, this step can be seen as more exploratory. The process is terminated if the last 5 iterations the objective function changes less than $1e^{-5}$. In a third step, the trust region samples parameter combination in the region of the current minimum to reach a better estimation of the local optimum. Here, the iterations are stopped if the last 5 iterations change the objective function less than $1e^{-5}$.

The multi-fidelity optimization is realized by the hierarchical kriging [5]. The method leads to an efficient creation of a surrogate model for the optimization. In general, the trend of a kriging model is given by low-order polynomials whereas the trend for the hierarchical kriging the trend is given by a lower-fidelity kriging model.

In the following diagram, see Fig 4, the structure of the optimization is shown. The outer SBO optimizes the lift to drag ratio L/D by changing the wing bending b and the design Mach number M_d . The design parameter can be varied as follows, $b \in [-0.6, 0.6]$ and $M_d \in [8, 14]$. The maximum L/D for the given b and M_d combination by the outer SBO is calculated by an inner SBO. As the stacked symbols highlight, the inner SBO exists in different fidelity levels, low-fidelity and multi-fidelity.

First the low-fidelity loop. The inner SBO starts the generation of the geometry which is held in-memory. This geometry is used to create an structured quadrilateral surface mesh for the panel solver. The flaps

are integrated by a mesh block of the size of the flaps. This mesh is handed to the low-fidelity flow solver in-memory. The flap deflections are archived by rotating the quadrilaterals w.r.t. the hinge lines. Here, the parameters are bounded by $\alpha \in [-15^\circ, 15^\circ]$, $\delta_{\text{luv}} \in [0, 25^\circ]$ and $\delta_{\text{lee}} \in [0, 25^\circ]$. Thereafter, the flow solution is calculated. The values for L/D and C_m feed back to the inner SBO, where the L/D is the objective and the C_m with a tolerance of $\pm 1e^{-4}$ is a constraint for feasible solutions. The values marked with the * are the current best output values.

Second the multi-fidelity loop. Here, the inner SBO can decide if the underlying trend of the low-fidelity surrogate needs to be improved or higher fidelity solutions are needed. If a low-fidelity solution is performed, the same loop as described above is used. Otherwise, the higher fidelity calculation is performed. Therefore, the geometry generation writes the geometry as IGES-file where the flaps are cut out of the geometry. The flaps are deflected as given by the SBO. The mesh is generated and stored as HDF5-file for the flow solver TAU. The solution is calculated and returned to the inner SBO.

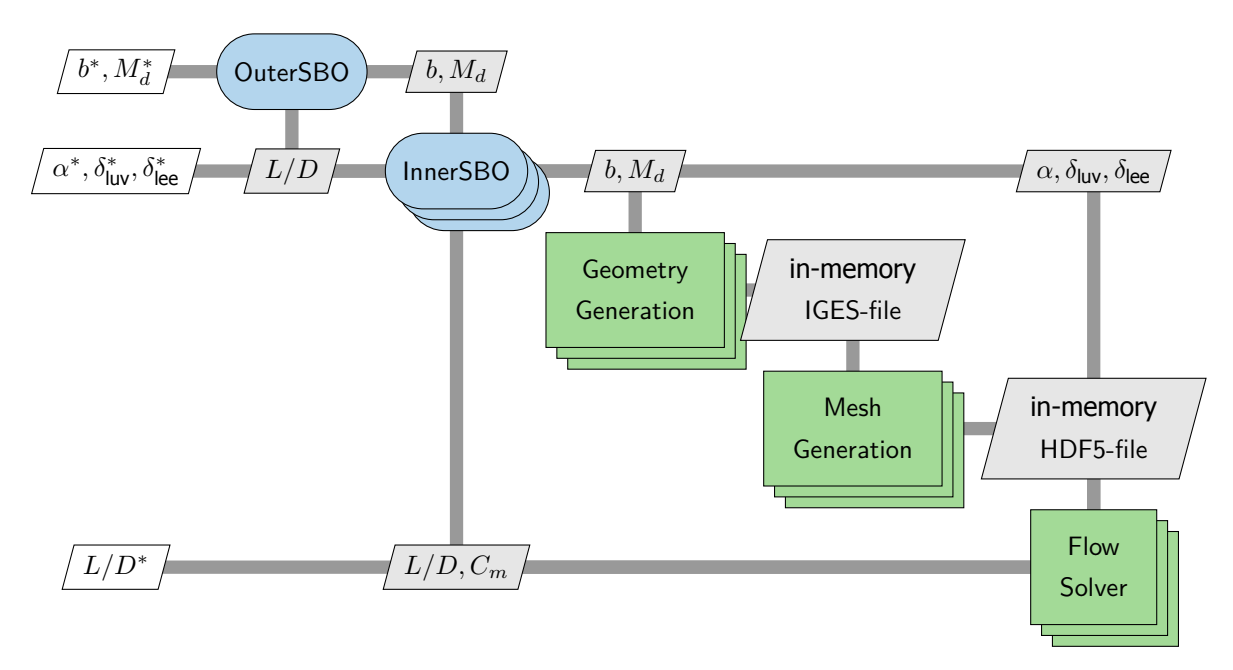


Fig 4. The structure of the SBO optimization.

3. Results

In the following section, the results of the single low-fidelity optimization and the multi-fidelity optimization are shown. First, the single low-fidelity results. In the following figure, see Fig 5, the outer surrogate is depicted. The lift to drag ratio is illustrated as colored contour plot whereas the estimated error is represented as isolines. In most of the surrogate, the error of the estimated lift to drag ratio is $L/D \pm 0.45$. The strong gradients in the error shows the points where data are provided by the inner SBO. Local minima and maxima can be seen in the region for the design Mach number $M_d > 9$. These values are mainly generated by the initial sampling. The clustering in the upper left of the plot, is the sampling by the expected improvement and the trust region. Here, the sampling is clustered, hence, the error is low and a global optimum forms. The black point marks the best value with $L/D^* = 5.9$ at $M_d^* = 8$ and $b^* = 0.327$. The inner surrogate SBO returned the following flight attitude: $\alpha^* = -0.52^\circ$, $\delta_{\rm lee}^* = 7.93^\circ$ and $\delta_{\rm luv}^* = 1.67^\circ$.

The Fig 6 shows the iterative sampling process of the SBO. The lift to drag ratio and the design parameter are plotted over the outer iterations i_o . The initial value results from the current best of the Sobol's sequence sampling. The design Mach number converges fast against the boundary of the parameter space to $M_d^*=8$. The wing bending increases for the first five iterations. Thereafter, the value of

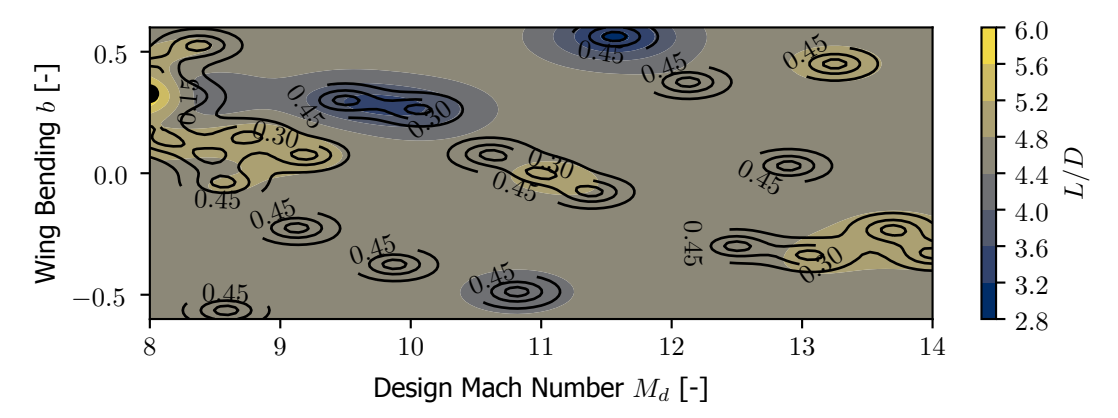


Fig 5. The outer surrogate of the low-fidelity optimization with the lift to drag ratio as contour and the estimation error as isolines.

the wing bending converges to $b^*=0.327$. Here, the best lift to drag ratio is $L/D^*=5.9$ as seen in the corresponding surrogate in Fig 5. The process ends after $i_o=14$ by reaching the convergence criteria.

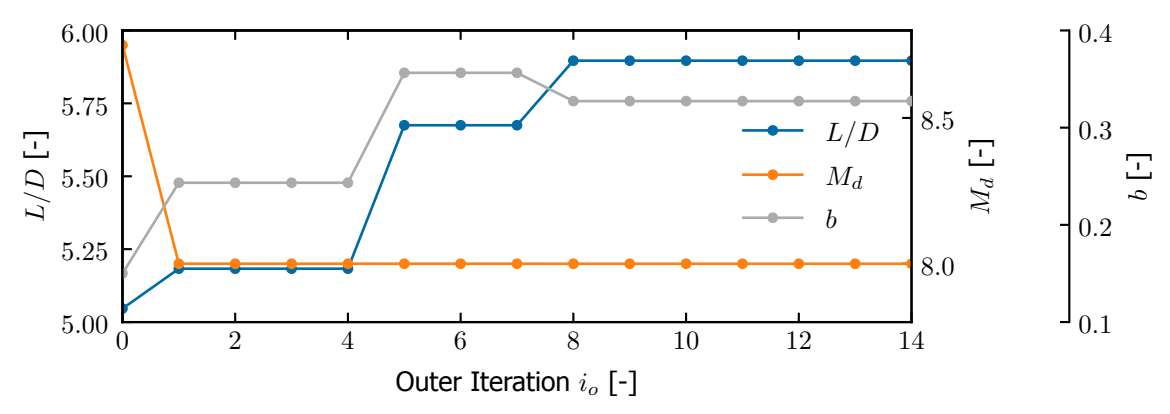


Fig 6. The lift to drag ratio and design parameter over the outer iterations i_o .

In the following, the preliminary results for the multi-fidelity optimization are shown. The results shall be seen as work in progress. The Fig 7 depicts the outer surrogates of the multi-fidelity optimization. As for the low-fidelity optimization results, the lift to drag ratio is depicted as contour and the estimation error as isolines. The Fig 7(a) shows the same trend as the one for the single low-fidelity optimization in Fig 5. This should be the case due to the same modelling. Thus, the optimum of the region of $M_d \approx 8.5$ and a wing bending of $b\approx 0.5$. The overlaying multi-fidelity model is plotted in the Fig 7(b). Here, it can be seen, the estimated error of the surrogate is very high, up to ± 8 in lift to drag ratio. Moreover, the lift over drag ratio is far different then the values of the low-fidelity surrogate. The range of the lift to drag ratio is approximately $L/D\approx -60$ to 45 which is not reasonable for a WR configuration. Due to the strong gradients in lift to drag, the expected improvement and trust region iterations directly converge to the best value of the initial sampling. The parameter combination of the current best $L/D^*=40.97$ is $M_d^*=9.5$, $b=0.3^*$, $\alpha^*=11.25^\circ$, $\delta_{\rm lee}^*=21.88^\circ$ and $\delta_{\rm luv}^*=3.13^\circ$. This is the reason of convergence problems of the inner multi-fidelity SBO.

Multiple problems within the multi-fidelity SBO lead to the bad convergence. The automatic generation of a suitable mesh for all combinations of geometric parameter, angle of attack and flap deflection is complex. Here, the mesh generation can fail or negatively influence the flow calculation. The mesh quality could be improved by mesh adaptation which would further leads to better compression shock

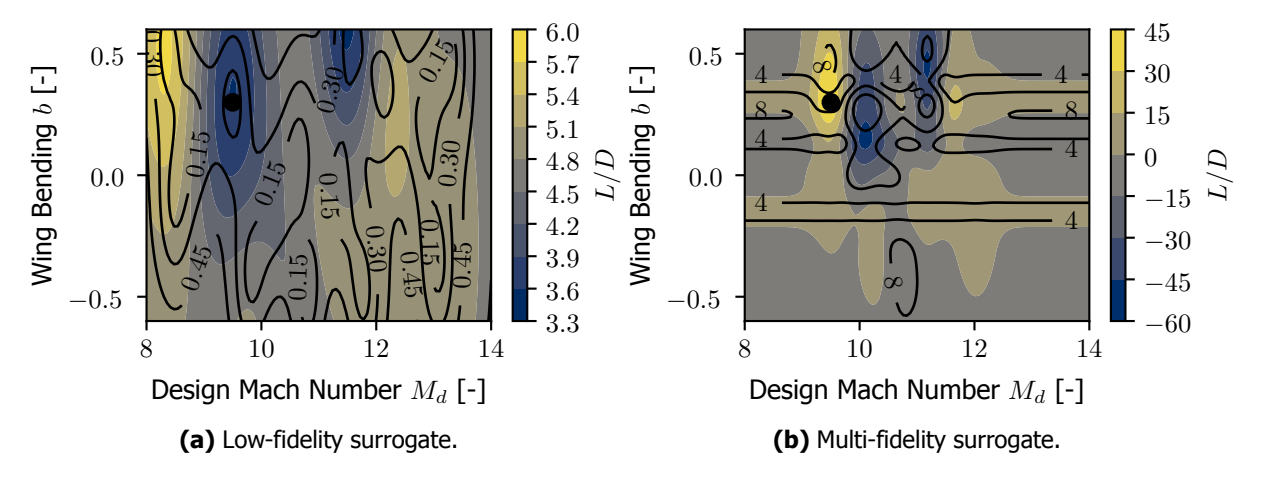


Fig 7. The outer surrogates of the multi-fidelity optimization with the lift to drag ratio as contour and the estimation error as isolines.

resolution and position. Furthermore, the gaps between the flaps and the body within the Euler calculations lead to complex flows which can cause instabilities within the calculation or abort the calculation. The gaps could be closed by using mesh deformation for the deflection of the control surfaces. These failures lead to non-filled parameter combinations. The failure of the solver can be handled by the SBO. If this happens too often in the optimization, no current best value can be evaluated and the optimization fails.

4. Conclusion

The present study shows preliminary results of the usage of multi-fidelity SBO for the shape optimization of WR shaped re-entry vehicle. The single low-fidelity optimization shows a converged solution for the cruise flight mission. The result is a WR with a lift to drag ratio of L/D=5.9. Further, the associated inner loop SBO yielded a trim-feasible flight attitude ($\alpha^*=-0.52^\circ$, $\delta^*_{\text{lee}}=7.93^\circ$, $\delta^*_{\text{luv}}=1.67^\circ$.) Herewith, the capability of the low-fidelity optimization is shown of exploring and identifying promising parameter combination.

The multi-fidelity optimization exposed several practical challenges. The higher fidelity calculations suffered from frequent failures within the mesh generation and convergence of the Euler calculations. Consequently, the estimated values show an non-realistic range of the lift to drag ratio $L/D\approx-60$ to 45. Due to a strong global optimum within the initial sampling and not converging inner SBO, the expected improvement and trust region sampling prematurely converges near the initial sampling. This shows, that the advantage of the multi-fidelity approach arises only if the higher fidelity methods can reliably fill the design space.

Future work will therefore focus on the improvement of the robustness of the higher fidelity calculations. This includes the mesh generation, mesh quality, mesh adaptation and reduction of the flap gap by e.g. mesh deformation.

5. Conflict of interest

No conflicts of interest were identified.

References

- [1] J. D. Anderson Jr. *Hypersonic and High-Temperature Gas Dynamics, Second Edition*. American Institute of Aeronautics and Astronautics, Reston ,VA, 2006. https://doi.org/10.2514/4.861956.
- [2] P. Bekemeyer, A. Bertram, D. A. H. Chaves, M. D. Ribeiro, A. Garbo, C. S. Campomanes, M. Stradt-

- ner, S. Wassing, M. Widhalm, S. Görtz, F. Jäckel, R. Hoppe, and N. Hoffmann. Data-Driven Aero-dynamic Modeling Using the DLR SMARTy Toolbox. In *AIAA Aviation 2022 Forum*, 2022.
- [3] F. Di Fiore, P. Maggiore, and L. Mainini. Multifidelity domain-aware learning for the design of re-entry vehicles. *Structural and Multidisciplinary Optimization*, 64(5):3017–3035, Nov. 2021. https://doi.org/10.1007/s00158-021-03037-4.
- [4] M. Franze and F. Barz. Flight stability analysis and flap size optimization along a trajectory of a waverider concept. In *HiSST: 4th International Conference on High-Speed Vehicle Science Technology*, Tours, France, Sept. 2025.
- [5] Z.-H. Han and S. Görtz. Hierarchical Kriging Model for Variable-Fidelity Surrogate Modeling. *AIAA Journal*, 50(9):1885–1896, Sept. 2012. https://doi.org/10.2514/1.J051354.
- [6] S. G. Kontogiannis, J. Demange, A. M. Savill, and T. Kipouros. A comparison study of two multi-fidelity methods for aerodynamic optimization. *Aerospace Science and Technology*, 97:105592, Feb. 2020. https://doi.org/10.1016/j.ast.2019.105592.
- [7] J. L. Loeppky, J. Sacks, and W. J. Welch. Choosing the Sample Size of a Computer Experiment: A Practical Guide. *Technometrics*, 51(4):366–376, Nov. 2009. https://doi.org/10.1198/TECH.2009.08040.
- [8] S. Mondal, M. M. Joly, and S. Sarkar. Multi-Fidelity Global-Local Optimization of a Transonic Compressor Rotor. In *Volume 2D: Turbomachinery*, page V02DT46A020, Phoenix, Arizona, USA, June 2019. American Society of Mechanical Engineers. https://doi.org/10.1115/GT2019-91778.
- [9] D. Schwamborn, T. Gerhold, and R. Heinrich. THE DLR TAU-CODE: RECENT APPLICATIONS IN RESEARCH AND INDUSTRY. In *ECCOMAS CDF*, 2006.
- [10] H. Sobieczky, F. C. Dougherty, and K. Jones. Hypersonic Waverider Design from Given Shock Waves. In *First International Waverider Symposium*, 1990.
- [11] I. M. Sobol. On the distribution of points in a cube and the approximate evaluation of integrals. *USSR Computational Mathematics and Mathematical Physics*, 7(4):86–112, Jan. 1967. https://doi.org/10.1016/0041-5553(67)90144-9.
- [12] S. Stappert, S. Callsen, and D. M. Sippel. Re-entry and Flight Dynamics of a Winged Reusable First Stage. In 9th European Conference on Aeronautics and Space Sciences (EUCASS), 2022.